Journal of Luminescence 198 (2018) 163–170

Contents lists available at ScienceDirect

Journal of Luminescence

journal homepage: www.elsevier.com/locate/jlumin

Temperature dependence of $4f^{n-1}5d^1 \rightarrow 4f^n$ luminescence of Ce^{3+} and Pr^{3+} ions in Sr_2GeO_4 host

Karolina Fiaczyk[a], Shun Omagari[b], Andries Meijerink[b], Eugeniusz Zych[a,*]

[a] Faculty of Chemistry, University of Wroclaw, 14. F. Joliot-Curie Street, 50-383 Wroclaw, Poland
[b] Department of Chemistry, Utrecht University, Princetonplein 1, 3584 CC Utrecht, The Netherlands

ARTICLE INFO

Keywords:
Thermal quenching
d→f luminescence
Pr3 +
Ce3 +
Strontium germanate

ABSTRACT

Photoluminescence of Ce^{3+}- and Pr^{3+}-activated Sr_2GeO_4 powders was measured between 17 and 600 K. For both ions strong $4f^{n-1}5d^n \rightarrow 4f^n$ (d-f) emission is observed at low temperatures, around 410 nm (Ce^{3+}) and 280 nm (Pr^{3+}). The Ce^{3+} d-f emission quenches starting at 150 K and disappearing completely just above room temperature. Pr^{3+} d-f luminescence shows an onset of quenching also around 150 K and disappears completely between 250 and 300 K. For Pr^{3+} quenching of the d-f emission was connected with an increasing intensity of the $^3P_0$ luminescence at first and $^1D_2$ emission at even higher temperatures. Both these $4f^n \rightarrow 4f^n$ emissions were observed up to 600 K. Based on the similar quenching temperatures, thermally stimulated photoionization of the 5d electrons from 5d level of Ce^{3+} or Pr^{3+} to the conduction band is proposed as the most probable mechanism for quenching of the d-f emissions.

1. Introduction

Orthosilicates doped with lanthanide ions form an important class of luminescent materials and Eu^{2+} doped Sr_2SiO_4 is known for application in white light LEDs (WLEDs). The thermal quenching temperature is however low (below 400 K) which prevents application in high power LEDs. The thermal quenching mechanism is possibly related to thermally activated photoionization. We recently reported on Eu^{2+} luminescence in Sr_2GeO_4 showing emission in the red spectral region around 620 nm [1]. The emission wavelength in the red is favorable for application in WLEDs but we have shown that the luminescence of Eu^{2+} suffered from strong thermal quenching starting already around 30 K. This observation is consistent with thermally activated photoionization. The bandgap of germanates is smaller than for silicates and the lower energy position of the conduction band can explain the lower temperature at which quenching by photoionization starts. According to Dorenbos model [2,3], the ground states of triply ionized lanthanides are positioned energetically much lower than the ground state of Eu^{2+}. Based on this and the low energy position of the Eu^{2+} d-f emission this opened question about possibility of generation of 5d→4f luminescence from Sr_2GeO_4:Ce^{3+} and Sr_2GeO_4:Pr^{3+}. This paper reports on the observation of d-f emission and the thermal quenching behavior of d-f emission from both these ions in Sr_2GeO_4.

The Sr_2GeO_4 host has a different crystal structure than Sr_2SiO_4. It offers four different symmetry sites, as depicted in Fig. 1. The lanthanide dopants are expected to occupy the different positions and show different luminescence spectra. Yet, while in the case of Eu^{3+} [1] and its f-f transitions multi-site luminescence was indeed observed, reduced samples showing broad band emission from Eu^{2+} did not have indications for luminescence from Eu^{2+} on multiple sites. The similarity in coordination for the four sites probably gives rise to overlapping emission bands resembling emission from Eu^{2+} on a single-site [1].

2. Experimental details

2.1. Synthesis

Ce^{3+} and Ce^{3+},Na^+ co-doped strontium germanate (Sr_2GeO_4) microcrystalline powders were prepared by standard solid state synthesis methods. Stoichiometry of the starting materials was formulated assuming that the dopants substitute strontium ions in the host lattice. Concentrations of cerium and sodium ions were 0.1, 0.5 and 1.0 mol%. Sodium ions were added to compensate the charge of Ce^{3+} on a Sr^{2+} site by a Na^+ ion on the Sr^{2+} site. The starting materials, $SrCO_3$, GeO_2, CeO_2, and Na_2CO_3, were thoroughly mixed and ground in an agate mortar, transferred to an alumina boat and heated at 1350 °C for 3 h in the reducing atmosphere of forming gas composed of 5%H_2 and 95%N_2. For samples doped with praseodymium the same procedure was used and concentrations of Pr^{3+} ions were: 0.05, 0.1, 0.5 mol%. Pr

* Corresponding author.
E-mail address: eugeniusz.zych@chem.uni.wroc.pl (E. Zych).

https://doi.org/10.1016/j.jlumin.2018.02.034
Received 15 September 2017; Received in revised form 6 February 2018; Accepted 8 February 2018
Available online 15 February 2018

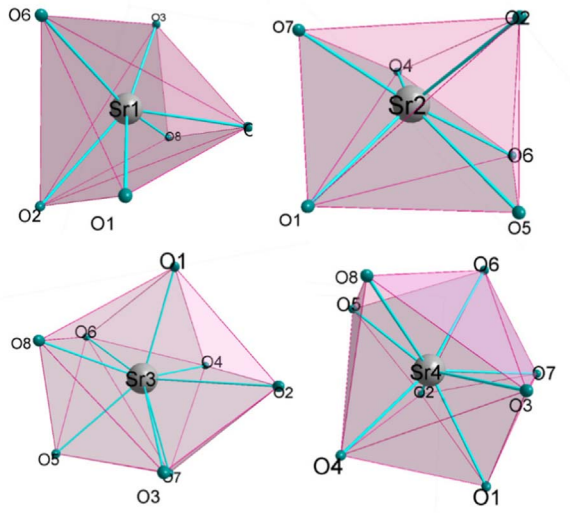

Fig. 1. Coordination sphere of different sites for Sr^{2+} in orthorhombic Sr_2GeO_4 [4].

$(NO_3)_3 \times 6H_2O$ was the source of the dopant.

2.2. Characterization

Photoluminescence (PL) and PL excitation spectra (PLE) were measured with an FLS980-sm Fluorescence Spectrometer from Edinburgh Instruments Ltd. using 450 W Xenon arc lamp as continuous excitation source. TMS302-X Single Grating excitation and emission monochromators of 30 cm focal lengths were used and the luminescence light was recorded by Hamamatsu R928P high-gain photomultiplier detector. Emission spectra were corrected for the wavelength dependence of the spectral response of the recording system and excitation spectra were corrected for the incident light intensity. The luminescence decay traces (DEC) were measured using the Edinburgh spectrofluorometer where pulsed excitation was done by means of EPLED-250 or EPLED-320 ps LEDs supplied by Edinburgh Instruments Ltd. The signal was registered by means of a F-G05 photomultiplier featuring a Hamamatsu H5773-04 detector. To obtain information on phase purity, for all samples X-ray diffraction measurements were performed with a D8 Advance X-ray Diffractometer from Bruker in the range of $2\theta = 0$–80° and with the step of $2\theta = 0.01608^\circ$. Ni-filtered Cu $K_{\alpha 1}$ radiation ($\lambda = 1.540596$ Å) was utilized. The resultant representative patterns are presented in Fig. 2 together with a reference pattern for orthorhombic Sr_2GeO_4 (ICSD#83345 [4]). They prove that

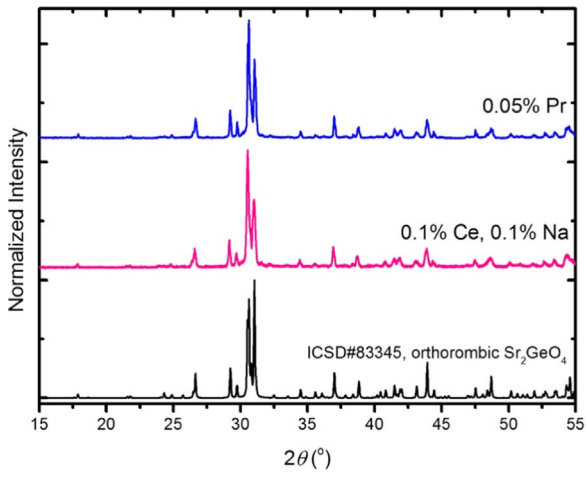

Fig. 2. X-ray diffraction patterns of Sr_2GeO_4:0.1%Ce,0.1%Na and Sr_2GeO_4:0.05%Pr prepared at 1350 °C in reducing atmosphere for 3 h.

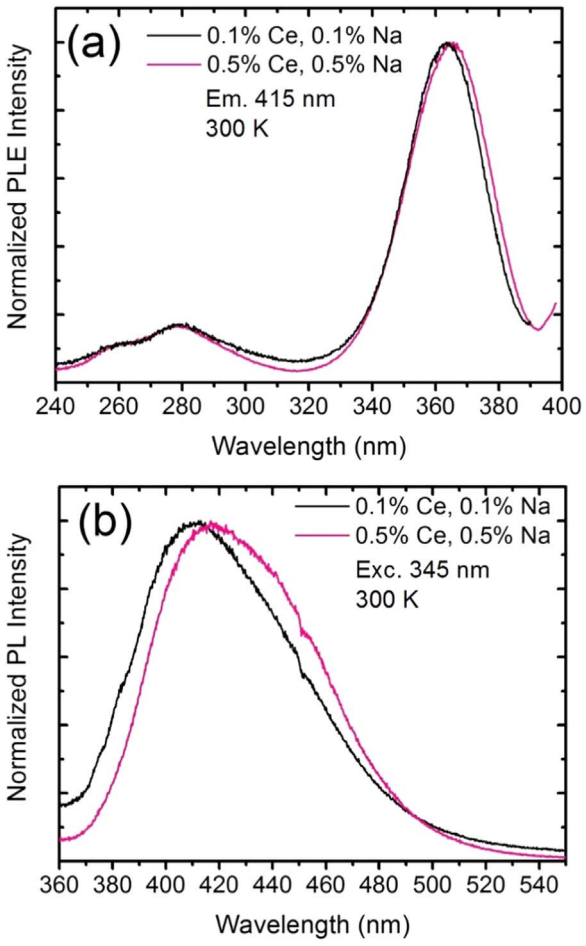

Fig. 3. PLE spectra of 415 nm emission of Sr_2GeO_4:Ce, Na powders with different content of dopants (a) and PL spectra under 345 nm excitation for the same samples (b). All spectra recorded at 300 K.

both Sr_2GeO_4:0.1%Ce,0.1%Na and Sr_2GeO_4:0.05% Pr are phase pure, orthorhombic materials.

3. Results and discussion

3.1. Photoluminescence of Sr_2GeO_4:Ce^{3+}

Luminescence measurements were performed for both Ce- and Ce-, Na-activated materials. No differences were observed between the spectra for the singly and co-doped materials except for a noticeably higher emission intensity for the Ce,Na co-doped powders. Below we present results for the co-doped phosphors only. Fig. 3a presents PLE spectra of Sr_2GeO_4:Ce,Na of emission at 415 nm for different contents of the dopant (0.1% and 0.5%) at 300 K. The concentration hardly affects the spectral shapes. The spectra consist of three bands peaking around 365 nm, 260 nm and 275 nm. The two latter bands overlap significantly. Fig. 3b shows the PL spectra of the same samples under 345 nm excitation. The spectra consist of a broad bands with a maximum around 415 nm. For the higher Ce content the emission is red-shifted (from 410 nm (0.1%) to ~ 418 nm (0.5%)). The red shift and the increase of intensity at the longer wavelength side in the more concentrated material is probably the result of reabsorption due to some overlap of the excitation and emission bands on the short wavelength side of the emission band. Alternatively, since the host offers four Sr sites which may all be occupied by Ce non-radiative energy transfer between Ce^{3+} ions may also play a role in shifting the emission to the red by energy transfer to Ce^{3+} ions with a lower energy 5d state which will be more efficient at higher Ce-concentrations. The characteristic ~

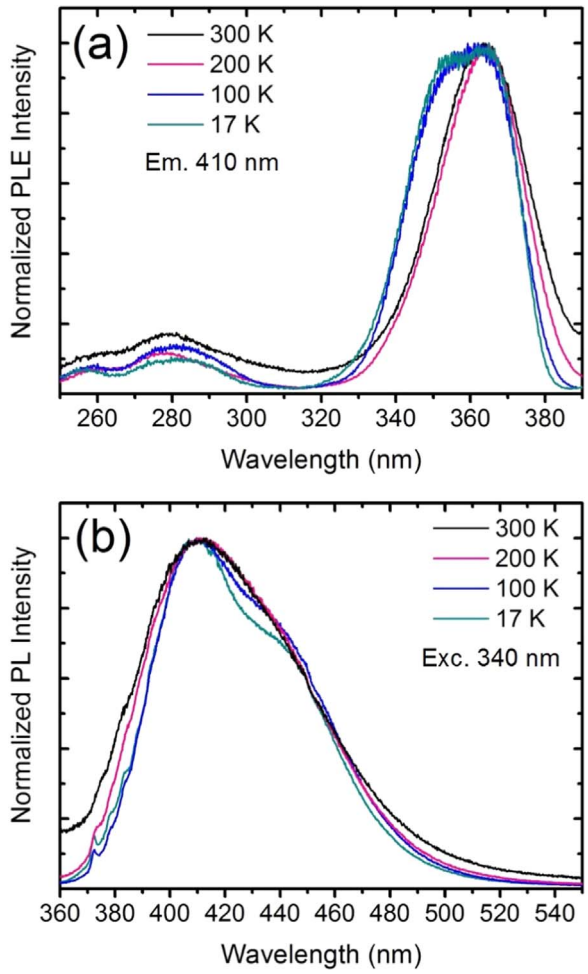

Fig. 4. PLE spectra of 410 nm emission of Sr_2GeO_4:0.1%Ce,0.1%Na (a) and PL spectra under 340 nm excitation (b) recorded at different temperatures indicated in the figure.

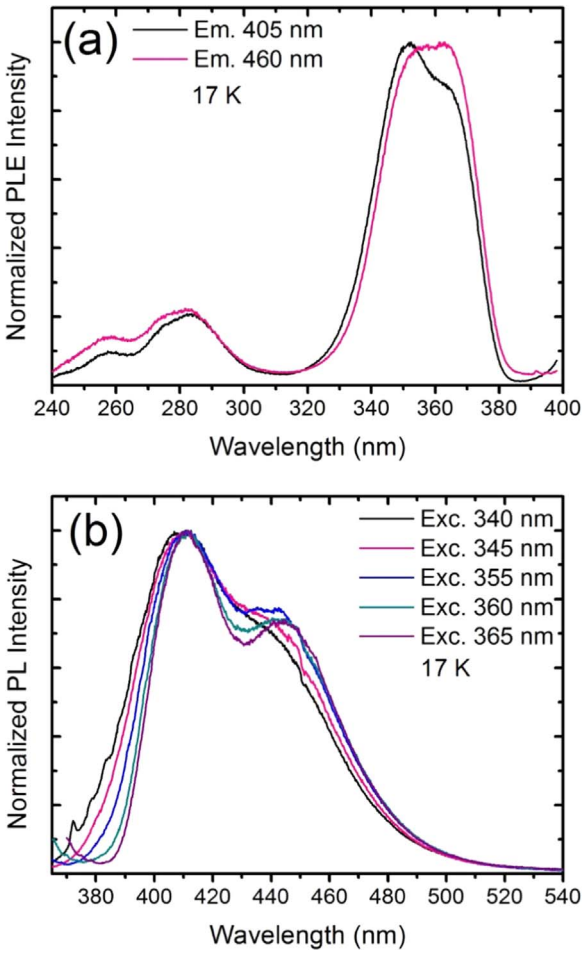

Fig. 5. PLE spectra of different emissions line for Sr_2GeO_4:0.1%Ce,0.1%Na recorded at 17 K (a) PL spectra taken upon different excitation wavelengths recorded at 17 K (b).

2000 cm^{-1} splitting of the Ce^{3+} luminescence bands due to transitions to the $^2F_{5/2}$ and $^2F_{7/2}$ levels of the $4f^1$ configuration is not clearly observed but the bands do show asymmetry connected with the ground splitting.

The photoluminescence spectra were further studied at various temperatures down to 17 K for the 0.1% sample (Fig. 4). With decreasing temperature the most intense excitation band (Fig. 4a) peaking around 360 nm broadens on the short-wavelength side. This indicates that Ce^{3+} ions having absorption in this spectral region are quenched at room temperature and start to show luminescence upon cooling. Note that the broadening of the band ~ 360 nm at low temperatures causes its maximum to span a wider wavelength range of ~ 355–365 nm and the band seems to be composed of two strongly overlapping components. This further support the conclusion that this absorption results from Ce^{3+} ions on different crystallographic sites and slightly shifted positions of their energy levels. The position and shape of bands with maxima at 260 and 275 nm do not show any changes with temperature indicating that these levels overlap more strongly for the different Ce^{3+} sites. The emission spectra show only minor changes with decreasing temperature as shown in Fig. 4b. The emission is in the 370–500 nm region. At lower temperatures the characteristic splitting of the two components due to the $5d^1 \rightarrow {}^2F_{5/2}, {}^2F_{7/2}$ transitions is observed. The effect is not as clearly observed as in other crystalline materials [5–9], which may be the result of overlapping emission bands from Ce^{3+} on the four different sites in Sr_2GeO_4.

To obtain further insight in the variation of luminescence properties for Ce^{3+} on the different sites luminescence spectra were recorded for different emission/excitation wavelengths. The PLE spectra at 17 K recorded monitoring the emission at its long- and short-wavelength sides as well as PL spectra taken upon excitation at the long- and short-wavelength sides of the main excitation band are depicted in Figs. 5a and 5b. The emission spectra (Fig. 5b) show only minor changes with excitation wavelength. The splitting of the two components becomes more pronounced upon longer wavelength excitation and there is broadening on the high-energy side for excitation at shorter wavelengths. The excitation spectra (Fig. 5a) for different emission wavelength show a change in the relative contributions for the shorter and longer wavelength component of two strongly overlapping components peaking around 350 nm and 365 nm. The excitation band maximum of the shorter wavelength emission (405 nm) is at 350 nm and for the longer wavelength emission (460 nm) intensities of the two components are almost identical. Based on these observations we conclude that the energy levels for Ce^{3+} on the different crystallographic Sr-sites discussed in Introduction, are slightly different and give rise to subtle variations in emission spectra for different excitation wavelengths. This is in line with previous observations for $Sr_2GeO_4:Eu^{2+}$ [1] where no clear difference was observed for Eu^{2+} on different sites.

The Ce^{3+} luminescence results from transitions to two $4f^1$ states, $^2F_{5/2}$ and $^2F_{7/2}$, which are typically separated by 2200–2300 cm^{-1} [10,11]. To obtain a quantitative estimate of the splitting the low temperature (17 K) emission spectrum was fitted with two Gaussian components and the results are presented in Fig. 6 and Table 1. The splitting between the two components is ~ 2045 cm^{-1} which is very close to expected value.

The 5d→4f emission of Ce^{3+} in Sr_2GeO_4 spans the violet-blue

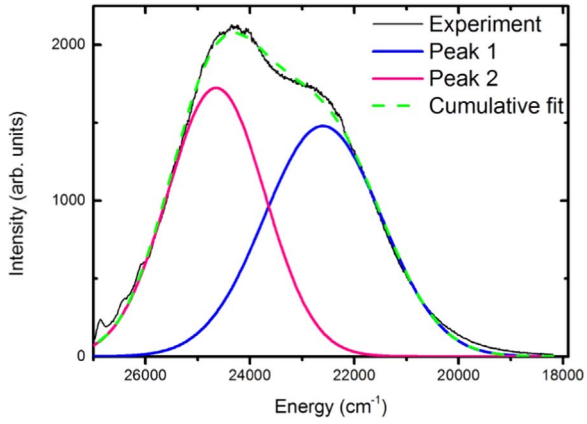

Fig. 6. Fitting of the Sr_2GeO_4:0.1% Ce emission at 17 K with two Gaussian components representing transitions from the lowest 5d level to the $^2F_{5/2}$ and $^2F_{7/2}$ levels of the $4f^1$ configuration of Ce^{3+}.

Table 1
Parameters of two Gaussian components to fit the emission spectra of Sr_2GeO_4:0.1%Ce as shown in Fig. 6.

Composition	Peak #1 (cm^{-1})	FWHM (cm^{-1})	% of Total PL	Peak #2 (cm^{-1})	FWHM (cm-)	% of Total PL
.1% Ce, 0.1% Na	24645	2197	49	22600	2641	51

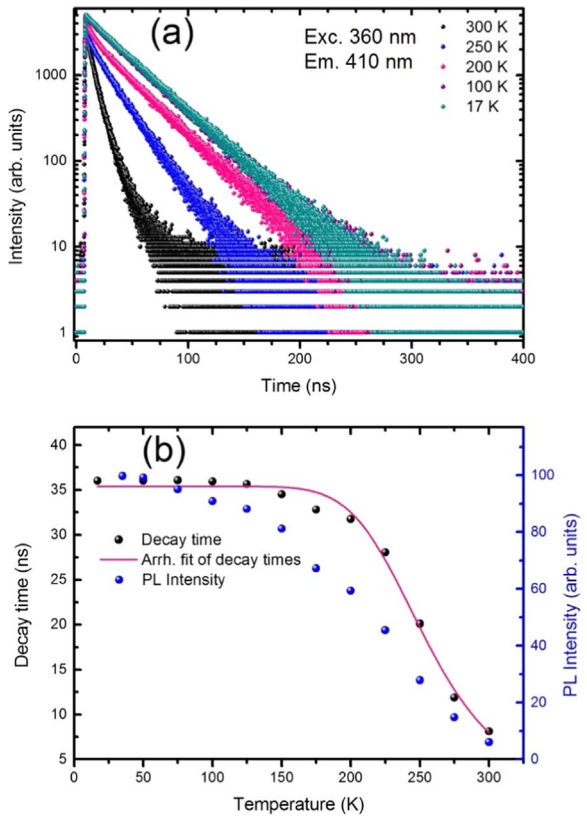

Fig. 7. Luminescence decay curves of Ce^{3+} emission in Sr_2GeO_4:0.1%Ce,0.1%Na between 17 and 300 K. Luminescence was monitored at 410 nm and excited at 360 nm (a), temperature dependence of the integrated photoluminescence intensity – blue circles (exc. 365 nm, em. 410 nm) and decay times – black circles, and the fit according to Eq. (1) - pink line (b).

spectral range and the material may be interesting for application in near-UV excited white LEDs (Near-UV WLEDs) although the excitation wavelength of 365 nm is shorter than that of present Near-UV WLEDs (380–410 nm). For application in WLEDs it is important to verify the temperature dependence of the emission and measure its quenching temperature. In Fig. 7 the temperature dependence of the luminescence decay time as well as that of the integrated emission intensity are shown. The decay time and intensity show a similar trend: both decrease strongly between 150 and 300 K. For a luminescent ion with a radiative decay rate p_R that is not strongly temperature dependent this is the signature of thermal quenching of luminescence. As the non-radiative decay rate p_{NR} increases, the emission intensity ($p_R/(p_R+p_{NR})$) and luminescence life time ($1/(p_R+p_{NR})$) both decrease in the same way with temperature. As discussed, there may be a difference in quenching temperature T_Q for Ce^{3+} on the different crystallographic sites with a slightly lower T_Q for Ce^{3+} ions emitting at shorter wavelength (see discussion on Fig. 4 above). This will lead to a multi-exponential decay behavior in the temperature range where the thermal quenching for different Ce^{3+} ions is different. The decay traces of the Ce^{3+} emission at different temperatures are shown in Fig. 7a and show single exponential character up to about 150 K with time constants of ~ 35–36 ns. At higher temperatures the traces depart from single exponential dependence consistent with differences in quenching behavior of Ce^{3+} on different sites. The average decay time shortens while the emission intensity drops (Fig. 7b). Parameters resulting from fitting of the decay traces are presented in Table 2. The d-f emission of Ce^{3+} is thermally quenched at temperatures higher than the for Eu^{2+} [1], but its relatively low quenching temperature excludes application of Sr_2GeO_4:Ce in (solid state) lighting.

A possible mechanism for the Ce^{3+} luminescence quenching is thermally activated photoionization [12–15]. The bandgap of germanates is smaller than for silicates which puts the lowest 5d state closer to the conduction band edge than in silicates. From the temperature dependence of the decay times of Ce^{3+} luminescence, see Fig. 7b, the activation energy (E_a) for the thermal quenching was calculated using the Arrhenius-type dependence given by Eq. (1) [16–18]:

$$p = \frac{1}{\tau} = \frac{1}{\tau_0} + B\exp\left(\frac{-\Delta E_a}{kT}\right) \quad (1)$$

where p (s^{-1}) and τ are the luminescence transition rate (p_R+p_{NR}) and decay time ($1/(p_R+p_{NR})$) at temperature T, respectively. τ_0 is radiative decay time ($1/p_R$) which is observed in the absence of quenching at low temperatures, B is a constant, ΔE_a is the energy activation for the quenching process (eV) and k is Boltzmann constant (8.6173×10^{-5} eV/K). The obtained value of $\Delta E_a = 0.19$ eV is higher than in the case of Eu^{2+} luminescence (0.029 eV) [1]. These data indicate that photoionization due to a proximity of the emitting 5d state of Ce^{3+} to the bottom of the host conduction band is responsible for the thermal quenching of Ce^{3+} luminescence in Sr_2GeO_4. To provide additional support for this explanation, below we discuss results on 5d→4f luminescence of Pr^{3+} in the same germanate host. If thermally activated

Table 2
Parameters derived from fitting decay traces of Sr_2GeO_4:0.1%Ce,0.1%Na 410 nm emission under 360 nm excitation in the 17–300 K range of temperatures using a bi-exponential function. Also the average decay time (depicted in Fig. 7(b) is determined from the best fits.

Temperature [K]	τ_1 [ns]	Rel_1%	τ_2 [ns]	Rel_2%	$<\tau>$ [ns]
300	13.0	40	5.3	60	8.1
250	21.4	93	2.1	7	20.1
200	33.9	93	4.1	7	31.7
150	34.5	100	–	–	34.5
100	36.0	100	–	–	36.0
50	36.0	100	–	–	36.0
17	36.0	100	–	–	36.0

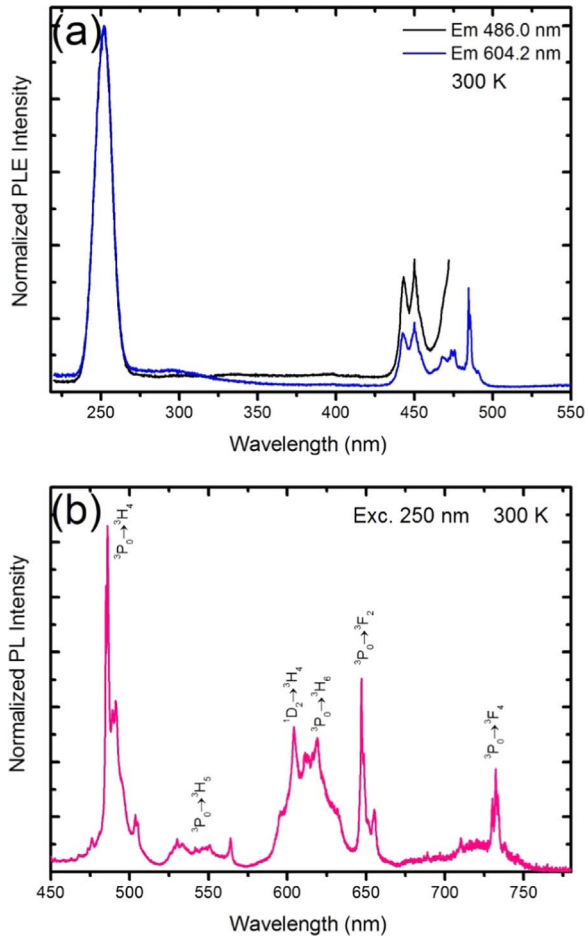

Fig. 8. Excitation spectra of 486.0 nm and 604.2 nm emission for Sr_2GeO_4:0.05% Pr (a) and emission spectra under 250 nm excitation for the same sample (b). Both spectra were recorded at 300 K.

photoionization is responsible, a similar quenching temperature is expected for the d-f emission of Ce^{3+} and Pr^{3+} as the energy difference of the lowest 5d state of trivalent lanthanides and the conduction band edge is expected to be similar. If the quenching is caused by thermally activated cross-over to the $4f^n$ states, a much lower T_Q is expected for d-f emission from Pr^{3+} as it has 4f states much closer in energy to the 5d state than Ce^{3+}.

3.2. Photoluminescence of $Sr_2GeO_4:Pr^{3+}$

We have researched both singly (Pr) and doubly doped (Pr,Na) powders. The former showed luminescence whose intensity was by ~ 10–15% higher compared to the latter. The temperature dependence of other luminescent properties of the two compositions was practically identical. Consequently, the data presented in this paper were specifically collected for $Sr_2GeO_4:Pr^{3+}$, but the overall conclusions are valid for both compositions.

Under circumstances where the relaxation from lowest 5d state to the highest $4f^2$ states ($^1I_6$, ^3P_J) of Pr^{3+} is slow, d-f emission can be observed for Pr^{3+} in the ultraviolet part of the spectrum. PLE and PL spectra for Sr_2GeO_4 doped with 0.05% Pr^{3+} and recorded at 300 K are presented in Fig. 8. The PLE spectrum in the visible consists of a series of excitation lines in the region of 420–500 nm that can be assigned to the $^3H_4 \rightarrow {}^3P_{0,1,2}$ transitions within the $4f^2$ configuration and a broad excitation band in the UV region with maximum at ~ 252 nm. This is at about 12,500 cm^{-1} higher energy than the first $4f \rightarrow 5d_1$ excitation 5d band of Ce^{3+} discussed above. This is exactly the energy difference that is expected between the 4f→5d excitation/absorption transitions of the two ions based on the constant energy difference between f-d absorption bands initially found by Blasse for Ce^{3+}, Pr^{3+} and Tb^{3+} and later generalized by Dorenbos for the 5d states of all lanthanide ions [19,20]. Thus, the 252 nm band is assigned to a transition from $^3H_4$ ground state to the lowest 5d level ($5d_1$) of Pr^{3+}. Excitation into this band at RT does not produce broad band UV emission which is characteristic of 5d→4f luminescence of Pr^{3+}. Only intense $4f^2 \rightarrow 4f^2$ luminescence of Pr^{3+} is observed at RT as shown in Fig. 8b. The emission spectrum consists of a series of narrow lines in the range of 450–750 nm which correspond to the $^3P_0 \rightarrow {}^3H_{4,5,6}$, $^3F_{2,3,4}$ and $^1D_2 \rightarrow {}^3H_{4,5}$ intraconfigurational $4f^2 \rightarrow 4f^2$ transitions. The assignments are given in Fig. 8b. The spin-allowed emission from $^3P_0$ level of Pr^{3+} dominates the spectrum at 300 K. The most intensive line from $^3P_0 \rightarrow {}^3H_4$ transition is located at 486.0 nm.

To learn more about the Pr^{3+} luminescence in $Sr_2GeO_4:Pr^{3+}$ a series of time resolved emission spectroscopy (TRES) experiments was performed at various temperatures. The results for 40 K, 300 K and 600 K are presented in Fig. 9 as TRES maps. At 40 K almost all lines related to the 4f→4f transitions have a short decay time of about 18 μs, a typical value for Pr^{3+} emission from the $^3P_0$ level. A more detailed analysis of the spectra and separately measured decay times at 40 K showed that one line of a very low intensity, located at 604.2 nm, is characterized by a longer decay time of 160 μs and can be ascribed to the $^1D_2 \rightarrow {}^3H_4$ transition. At 40 K intense broad band emission in UV region (~ 250–370 nm) is also observed. This band has a very short decay time that could not be resolved upon micro-second excitation pulses used in the TRES experiments. These results indicate that the luminescence may be due to d-f emission of Pr^{3+}. Below we will provide further evidence for this assignment. The room temperature TRES spectra in Fig. 9b show only $4f^2$-$4f^2$ line emission in the visible but no broad band emission in the UV. The $^3P_0$ emission is observed in the 480–750 nm region and the decay time of the various lines is $\tau = 18$ μs. At ~ 604 nm a longer decaying component is clearly seen in the TRES

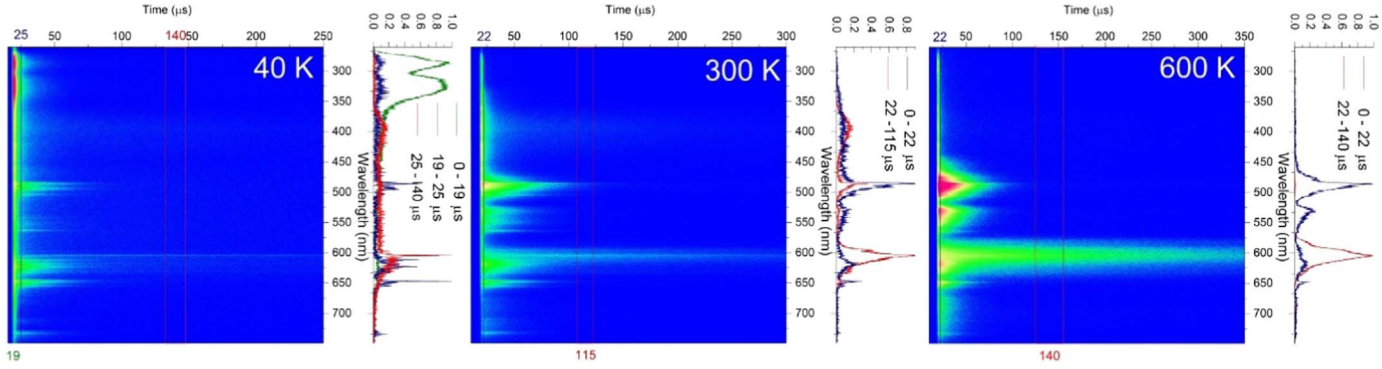

Fig. 9. Time Resolved Emission Spectroscopy (TRES) for Sr_2GeO_4:0.05% Pr under 250 nm excitation recorded at 40, 300 and 600 K. On the right hand side of the 2D plots spectra for different delay times after the excitation pulse are plotted.

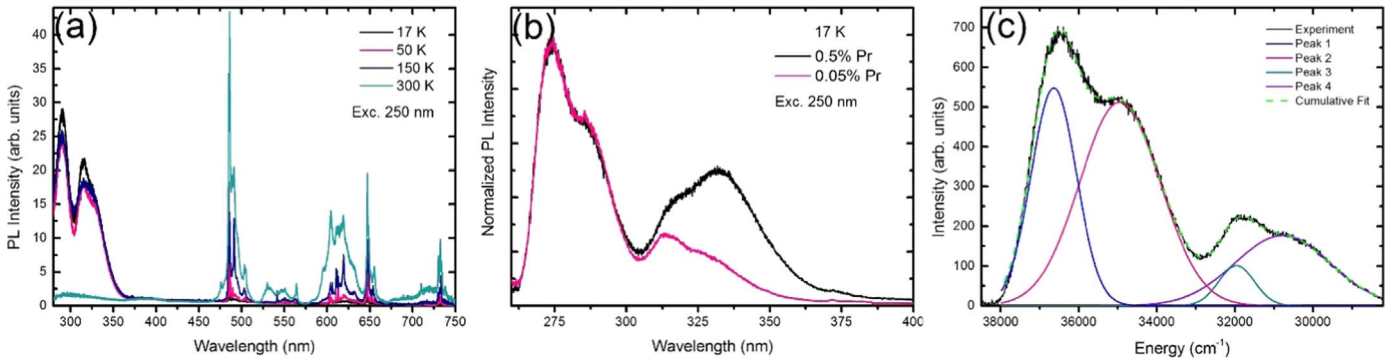

Fig. 10. PL spectra under 250 nm excitation for Sr_2GeO_4:0.05% Pr between 17 and 300 K (a) and the d-f emission of Pr^{3+} (λ_{exc} = 250 nm) for two Pr3 + concentrations: 0.05% and 0.5% (b), deconvolution of the Sr_2GeO_4:0.05% Pr emission spectra at 17 K into four Gaussian components representing transitions to ground levels of Pr^{3+}(c).

map although its contribution to the total emission is low. Comparison of PL spectra recorded with the delays of 22 μs and 115 μs (right part of Fig. 9b) clearly show their different spectral distributions. The $^1D_2$ emission is clearly observed for the longer 115 μs delay with a decay time τ = 164 μs. Increasing the sample temperature to 600 K (Fig. 9c) further increases the relative intensity of the $^1D_2$ luminescence compared to the $^3P_0$-related lines. Nevertheless, the latter emission is still observed proving its good resistance to thermal quenching.

Summarizing, the TRES data show that the $^3P_0$ emission is observed over the full range of investigated temperatures (17–600 K). With increasing temperature the $^1D_2$ emission intensity increases relative to the $^3P_0$ emission. Indications for 5d→4f luminescence in the UV were observed at 40 K.

To further investigate the presence of d-f emission and to obtain a better understanding of the temperature dependence of the Pr^{3+} emission, spectra were recorded at various temperatures down to 17 K. In Fig. 10a emission spectra of Sr_2GeO_4:0.05% Pr upon 250 nm excitation are shown for four different temperatures. Upon decreasing the temperature from RT to 150 K a broad band emission with maxima at 280 and 315 nm comes up and dominates the spectrum (Fig. 10a). Simultaneously, the intensity of narrow lines $4f^2$→$4f^2$ emission decreases. At 17 K emission from $^3P_0$ and $^1D_2$ levels of Pr^{3+} show only low intensity. Thus, the broad band UV and the 4f→4f emissions have a strong and opposite temperature dependence. Based on the spectral shape and position the UV broad band luminescence can be assigned to interconfigurational $4f^15d^1$→$4f^2$ transitions of Pr^{3+}. Also for the sample with higher Pr^{3+} concentration (0.5%) the 5d→4f emission of Pr^{3+} is observed at low temperatures (Fig. 10b). The difference with the 0.05% sample is that the relative contribution from the long-wavelength fraction (310–370 nm) is clearly higher. Stronger reabsorption of emission on the short wavelength side in the more concentrated sample can explain the change in intensity ratio.

For both concentrations of Pr^{3+} (0.05% and 0.5%) the 5d→4f emission bands at 17 K were fitted by four Gaussian components. Resultant data are summarized in Table 3. Result for 0.05% Pr is also presented in Fig. 10c. For both Pr^{3+} concentrations the positions of the respective four components are very similar. These four constituents represent four transitions from $4f^15d^1$ state of Pr^{3+} to $^3H_{4–6}$ and $^3F_{2–4}$ multiplets in the $4f^2$ configuration (see Table 3).

Table 3
Parameters of four Gaussian components and their assignment to appropriate transitions for Sr_2GeO_4:0.05% Pr and Sr_2GeO_4:0.5% Pr.

Maximum [cm^{-1}]	Peak 1	Peak 2	Peak 3	Peak 4
.05% Pr	36642	34947	31959	30786
0.5% Pr	36660	35010	31874	30105
Transition:	$4f^15d^1$→$^3H_4$	$4f^15d^1$→$^3H_5$	$4f^15d^1$→($^3H_6$,$^3F_2$)	$4f^15d^1$→($^3F_3$,$^3F_4$)

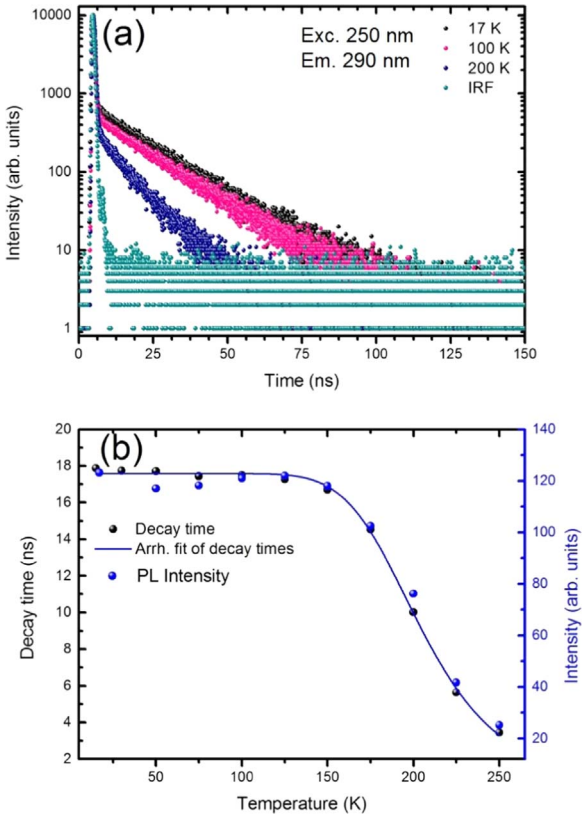

Fig. 11. Luminescence decay curves of d-f emission of Sr_2GeO_4:0.05%Pr for various temperature (exc. 250 nm, em. 290 nm) (a), temperature dependency of the photoluminescence intensity – blue circles (exc. 250 nm, em. 290 nm) and luminescence decay times – black circles and the fit according to Eq. (1) - blue line (b).

To further characterize the UV luminescence of Sr_2GeO_4:Pr^{3+} and luminescence quenching, both the integrated emission intensity and luminescence decay curves were measured at different temperatures. The results are presented in Fig. 11. All decay traces shown in Fig. 12a could be well fitted with single-exponential function. Fig. 11b presents the temperature dependence of the luminescence decay times and intensities. These curves ideally coincide, as discussed above, if the decay time is temperature independent which is the case here. Up to 150 K the 5d→4f luminescence is not quenched and the decay time is τ~ 17.5 ns which is typical for d-f emission from Pr^{3+} [21]. Above 150 K the decay time shortens and the luminescence intensity drops until the emission is completely quenched around 300 K. The fitting to the Arrhenius-type Eq. (1) gives the activation energy for thermal quenching of ΔE = 0.15 eV, ~ 0.04 eV less than the value we found in the case of Ce^{3+}.

The similarity in activation energies for thermal quenching of the d-

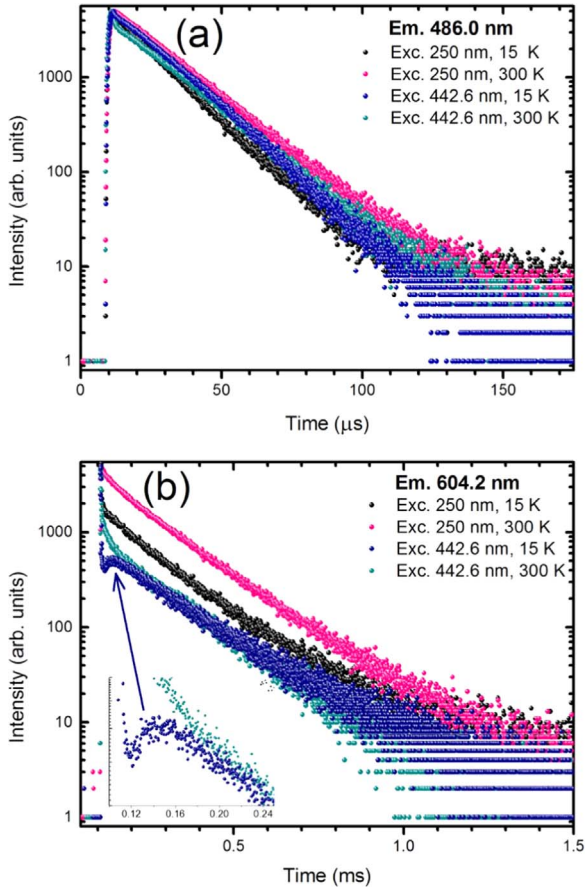

Fig. 12. Decay curves of $^3P_0$ (a) and $^1D_2$ (b) luminescence for Sr_2GeO_4 using two different excitation wavelength: 250 and 442.6 nm and recorded at 17 and 300 K.

f emission for Pr^{3+} and Ce^{3+} is expected if the quenching mechanism is thermally activated photoionization. In the Dorenbos model it has been argued that the position of the 5d state relative to the conduction band is very similar for all trivalent lanthanides (slightly decreasing towards the heavier lanthanides). In this situation, similar activation energies and thermal quenching temperatures are expected for photoionization from the lowest 5d state. For thermal quenching by thermal cross-over from the 5d excited state to 4f states, a much lower quenching temperature is expected (and has also been observed) for Pr^{3+} where the higher energy 4f states are much closer to the 5d states than for Ce^{3+}. Based on the similarity in quenching temperature and activation energy for Ce^{3+} and Pr^{3+} thermal quenching we conclude that thermally activated photoionization is responsible for the quenching. The small difference in quenching temperature could be due to a contribution of the other mechanism (thermally activated cross-over in the configurational coordinate diagram) which starts to contribute between 150 and 300 K. The observed increasing intensity of the 4f→4f transitions above 150 K shows there is feeding of the $4f^2$ excited states from the 5d state. A contribution from this second quenching channel can justify the complete absence of 5d→4f emission of Pr^{3+} at 300 K, when Ce^{3+} 5d→4f luminescence is still observed (albeit weak). Based on the analysis presented we have obtained a consistent picture of the luminescence quenching processes in both Sr_2GeO_4:Ce and Sr_2GeO_4:Pr. For both ions the 5d→4f emission is quenched starting at 150 K by thermally activated photoionization. For Ce^{3+} this is the operative mechanism while for Pr^{3+} it cannot be excluded that there is also a contribution from cross-over to the highest energy $4f^2$ states. The low thermal quenching temperatures are related to the low energy position of the conduction band in germanates. The observations also agree with the previously reported results for Sr_2GeO_4:Eu^{2+} where also quenching at very low temperatures was explained by photoionization from the $4f^65d^1$ state of Eu^{2+} to the conduction band [1].

Luminescence decay traces of the $^3P_0$ and $^1D_2$ emissions at different temperatures bring more information on energy relaxation processes in Sr_2GeO_4:Pr. In Fig. 12a the decay traces at 17 K and 300 K of the $^3P_0$ luminescence excited into the 5d band (~ 250 nm) or into the $^3P_2$ lines (442.6 nm) are presented. Reasonable fits were obtained using single exponential functions combined with a deconvolution of the instrumental response function (IRF). The derived time constants were in the range of 15–18 μs. In the case of emission from $^1D_2$ level the situation is more complex as shown in Fig. 12b. At room temperature the trace upon the 250 nm 4f→5d excitation (pink dots) has decay time of τ = 165 μs, a value very similar to τ = 156 μs obtained under the $^3H_4$→$^3P_2$ 442.6 nm excitation (cyan dots). The situation changes at 17 K. Under 250 nm excitation (black dots) the decay time of the very weak $^1D_2$ luminescence is τ = 162 μs, so it does not differ from the RT value. Yet, upon the $^3H_4$→$^3P_2$ excitation at 442.6 nm the 17 K decay trace of the $^1D_2$ emission shows significant rise (build up) of the signal before it decays with a time constant derived from the fit being τ = 190 μs. The rise of the signal reflects a feeding by relaxation from the $^3P_0$ levels. On the other hand, the absence of a rise in the 17 K decay of the $^1D_2$ luminescence upon 250 nm excitation indicates that the nonradioactive $5d_1$→$^1D_2$ relaxation bypasses by the ^3P_J levels. Thus, nonradiative $^3P_0$→$^1D_2$ relaxation is not efficient and this explains why the $^3P_0$ emission is intense even at 600 K (see Fig. 9).

Based on the findings we present a schematic representation of the quenching mechanisms of the 5d→4f luminescence of Ce^{3+} and Pr^{3+} in Sr_2GeO_4 in Fig. 13. The crucial point is that the 5d emitting levels are located quite close to the bottom of conduction band for both ions. The thermal barrier for the 5d electrons to escape to the conduction band is ~ 0.19 eV for Ce an ~ 0.15 eV for Pr. As a result, starting around 150 K the 5d→4f emission of both the activators is quenched by a thermally activated photoionization as is shown in Fig. 13a (Ce) and 13b (Pr). In the case of Pr the quenching of the 5d→4f emission is accompanied by an increase of the 4f→4f luminescence. This proves that the excited 5d state relaxes to the $^3P_0$ or $^1D_2$ levels when the 5d→4f emission is quenched, see Fig. 13c. Then, the characteristic 4f→4f luminescence of Pr^{3+} is generated which is observed up to 600 K at least.

4. Conclusions

The optical properties and luminescence quenching of Ce^{3+} and Pr^{3+} luminescence in Sr_2GeO_4 were investigated. Both ions show 5d→4f emission at cryogenic temperatures. The violet-blue Ce^{3+} emission and the UV 5d→4f emission of Pr^{3+} quench at relatively low temperatures. Above 150 K quenching starts and at 300 K there is little

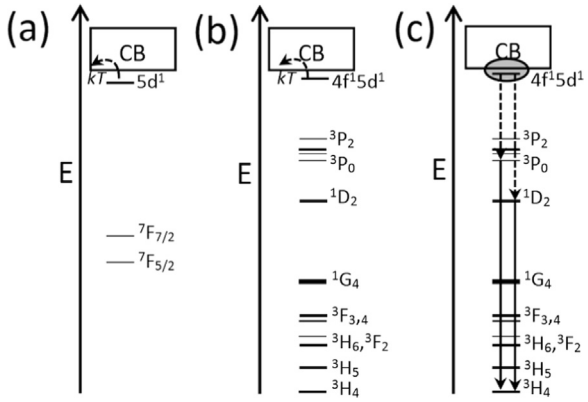

Fig. 13. Energy level diagrams for Ce^{3+} (a) and Pr^{3+} (b, c) in Sr_2GeO_4 showing quenching mechanisms of the d-f emissions of both dopants in this host. In Pr^{3+} not only quenching by photoionization (b), but also relaxation to the $^3P_0$ and $^1D_2$ levels occurs at higher temperatures (c).

(Ce^{3+}) or no (Pr^{3+}) d-f emission left. Based on the similar quenching temperatures, thermally active photoionization is identified as the prime quenching mechanism with activation energies of $\Delta E = 0.19$ eV (for Ce^{3+}) and $\Delta E = 0.15$ eV (for Pr). In the case of Pr the disappearance of the d→f luminescence is accompanied by an increase of $4f^2 \rightarrow 4f^2$ line emission from the $^3P_0$ and from $^1D_2$ states. Both these intraconfigurational emissions are observed up to at least 600 K. The low thermal quenching temperature of the d-f emission of Ce^{3+} and Pr^{3+} ions is related to the low energy position of the conduction band in germanates and is in line with the even lower thermal quenching temperature observed previously for Eu^{2+} d-f luminescence in this host.

Funding sources

This work was supported by Polish National Science Center (NCN) grant 2015/19/N/ST5/00637. Partial support under grant UMO-2017/25/B/ST5/00824 (NCN) and POIG.01.01.02-02-006/09 project co-funded by European Regional Development Fund within the Innovative Economy Program, Priority I, Activity 1.1. Subactivity 1.1.2 is also acknowledged.

References

[1] K. Fiaczyk, E. Zych, On peculiarities of Eu^{3+} and Eu^{2+} luminescence in Sr_2GeO_4 host, RSC Adv. 6 (2016) 91836–91845.
[2] P. Dorenbos, Energy of the first $4f^7 \rightarrow 4f^6 5d$ transition of Eu^{2+} in inorganic compounds, J. Lumin. 104 (2003) 239–260.
[3] P. Dorenbos, Systematic behaviour in trivalent lanthanide charge transfer energies, J. Phys. - Condens. Mat. 15 (2003) 8417–8434.
[4] F. Nishi, Y. Takeuchi, Structure of strontium germanate α'L- Sr_2GeO_4, Z. Krist. 211 (1996) 607–611.
[5] D. Kulesza, J. Cybinska, L. Seijo, Z. Barandiaran, E. Zych, J. Cybińska, et al., Anomalous red and infrared luminescence of Ce^{3+} Ions in SrS:Ce sintered ceramics, J. Phys. Chem. C 119 (2015) 27649–27656.
[6] E. Zych, D. Kulesza, J. Zeler, J. Cybińska, K. Fiaczyk, A. Wiatrowska, SrS:Ce and $LuPO_4$:Eu sintered ceramics: old phosphors with new functionalities, ECS J. Solid State Sc. Tech. 5 (2016) 3078–3088.
[7] H. Feng, Cerium concentration and temperature dependence of the luminescence of $Lu_2Si_2O_7$:Ce scintillator, J. Alloy. Compd. 509 (2011) 3855–3858.
[8] M. Kitaura, S. Tanaka, M. Itoh, Optical properties and electronic structure of Lu_2SiO_5 crystals doped with cerium ions: thermally-activated energy transfer from host to activator, J. Lumin. 158 (2015) 226–230.
[9] J.M. Ogiegło, A. Katelnikovas, A. Zych, T. Jüstel, A. Meijerink, C.R. Ronda, Luminescence and luminescence quenching in $Gd_3(Ga,Al)_5O_{12}$ scintillators doped with Ce^{3+}, J. Phys. Chem. A 117 (2013) 2479–2484.
[10] E.N. Willimas G M, P.C. Becker, J.G. Conway, L.A. Boatner, M.M. Abraham, Intensities of electronic Raman scattering between crystal-field levels of Ce^{3+} in $LuPO_4$: nonresonant and near-resonant excitation, Phys. Rev. B 40 (1989) 4132–4142.
[11] G.M. Williams, E. N, L.A. Boatner, M.M. Abraham, Anomalously small 4f-5d oscillator strengths and 4f-4f electronic Raman scattering cross sections for Ce^{3+} in crystals of $LuPO_4$, Phys. Rev. B 40 (1989) 4143–4152.
[12] G. Blasse, W. Schipper, J.J. Hamelink, On the quenching of the luminescence of the trivalent cerium ion, Inorg. Chim. Acta 189 (1991) 77–80.
[13] C. Pedrini, F. Rogemond, D.S. McClure, Photoionization thresholds of rare-earth impurity ions. Eu^{2+}:CaF_2, Ce^{3+}:YAG, and Sm^{2+}:CaF_2, J. Appl. Phys. 59 (1986) 1196–1201.
[14] J. Ueda, S. Tanabe, T. Nakanishi, Analysis of Ce^{3+} luminescence quenching in solid solutions between $Y_3Al_5O_{12}$ and $Y_3Ga_5O_{12}$ by temperature dependence of photoconductivity measurement, J. Appl. Phys. 110 (2011) 1–6.
[15] K.V. Ivanovskikh, J.M. Ogieglo, A. Zych, C.R. Ronda, A. Meijerink, Luminescence Temperature Quenching for Ce^{3+} and Pr^{3+} d-f Emission in YAG and LuAG, ECS J. Solid State Sci. Technol. 2 (2012).
[16] M. Yamaga, Y. Ohsumi, T. Nakayama, T.P.J. Han, Persistent phosphorescence in Ce-doped Lu_2SiO_5, Opt. Mater. Express 2 (2012) 413–419.
[17] J. Pejchal, M. Nikl, E. Mihokova, A. Novoselov, A. Yoshikawa, R.T. Williams, Temperature dependence of the Pr^{3+} luminescence in LSO and YSO hosts, J. Lumin. 129 (2009) 1857–1861.
[18] C.D.S. Brites, A. Millán, L.D. Carlos, Lanthanides in Luminescent Thermometry, Handbook on the Physics and Chemistry of Rare Earths 49 (2016), pp. 339–427.
[19] A.J. de Vries, G. Blasse, On the possibility to sensitize Gd^{3+} luminescence by the Pr^{3+} ion, Mater. Res. Bull. 21 (1986) 683.
[20] P. Dorenbos, 5D level positions of the trivalent lanthanides in inorganic compounds, J. Lumin. 91 (2000) 155–176.
[21] A. Zych, M. De Lange, C. De Mello Donegá, A. Meijerink, Analysis of the radiative lifetime of Pr^{3+} d-f emission, J. Appl. Phys. 112 (2012).